

pH-Responsive Fe(III)–Gallic Acid Nanoparticles for In Vivo Photoacoustic-Imaging-Guided Photothermal Therapy

Jianfeng Zeng, Ming Cheng, Yong Wang, Ling Wen, Ling Chen, Zhen Li,* Yongyou Wu,*
Mingyuan Gao,* and Zhifang Chai

Nanomaterials integrated with different therapeutic and diagnostic functional agents have attracted considerable attention in recent years due to their great potential in precision medicine.^[1] To date, large quantities of theranostic agents for simultaneous use in different imaging and therapeutic technologies, such as magnetic resonance imaging–photothermal therapy (MRI-PTT),^[2] optical imaging–photodynamic therapy,^[3] MRI-chemotherapy,^[4] computed tomography (CT)-PTT,^[5] and photoacoustic imaging (PAI)-PTT,^[6] were fabricated from individual functional agents, which could be detached from each other during circulation and metabolism in vivo, leading to different biodistributions and pharmacokinetics, inaccurate diagnosis, and poor therapy efficacy. Therefore, it is important to develop theranostic platforms based on single material which can serve as both imaging agent and therapeutic agent.^[7]

Near-infrared (NIR) absorbing materials have strong absorption in the region of 700–3000 nm. An advantage of this type of material is their capability of converting the NIR light, which can penetrate into deep tissues, into heat for PAI and thermal ablation of malignant tumors.^[5,6,8] PAI shows distinct advantages over the traditional optical imaging, including low signal scattering in tissues, and high resolution and sensitivity. PTT is a promising noninvasive alternative to traditional cancer therapies, which has attracted considerable interest in recent years

due to its highly specific selectivity towards the targeted sites. The combination of PTT and PAI could provide a perfect solution for accurate diagnosis and treatment of cancer, because they could both use the same NIR absorbing material as theranostic agent without any need to consider detachment of different functional units after intravenous administration.

The currently available NIR-absorbing materials include NIR dyes,^[9] gold nanomaterials,^[10] carbon nanomaterials,^[6,11] upconversion nanoparticles,^[12] transition-metal dichalcogenides,^[13] and some organic polymers.^[14] In comparison with small molecular NIR dyes, NIR absorbing nanomaterials with proper surface modification exhibit longer blood circulation time for tumor targeting. In addition, due to the enhanced permeability and retention (EPR) effect, nanomaterials also have longer retention time in tumor sites than small molecules, and provide a much longer time window for tumor diagnosis and therapy. Nevertheless, most exogenous nanomaterials are easily taken up by the reticuloendothelial system (RES), e.g., liver and spleen, which could cause potential risks of toxicity due to long retention time if they are difficult to degrade and metabolize in vivo. Therefore, the development of nanotheranostic agents that are subject to fast metabolism in normal organs and tissues, but have long retention time in tumors is of great importance for their practical applications.

Herein, we report a novel PAI–PTT theranostic agent based on pH-sensitive Fe(III)–gallic acid nanoparticles with strong NIR absorbance, which can be easily decomposed under neutral conditions, but remain stable under acidic conditions. Due to the weak acidic condition in tumors, which is different from that in normal tissue, our Fe(III)–gallic acid nanoparticles could be retained in tumor sites, while being easily decomposed and metabolized in other organs, leading to excellent in vivo photoacoustic imaging and a good photothermal therapy effect against tumors in mice.

It is well known that transition metal ions generally have incompletely filled *d* orbitals. When ligands bond to them to form complexes, the electrons in the ligands and the electrons in the *d* orbitals of metal ions interact with each other and induce splitting of the *d* orbitals, resulting in *d*–*d* electronic transitions and subsequent absorption of light under excitation. As the *d*–*d* transitions of metal ions strongly depend on the ligand properties, the absorbance of metal ion complexes can be adjusted in the UV–vis and even the NIR region by manipulating the ligands and their coordination chemistry. An example is Fe(III)–gallic acid complex with strong NIR absorbance prepared by simply mixing FeCl₃ solution with gallic acid solution, which features a bluish-violet color, as shown in **Figure 1a**, due to the *d*–*d* electronic transitions. The corresponding UV–vis–NIR absorption spectra display wide absorption from 400 to 900 nm, with a peak centered at 575 nm.

Dr. J. F. Zeng, Dr. Y. Wang, L. Wen, L. Chen, Prof. Z. Li,
Prof. Z. F. Chai
Center for Molecular Imaging and Nuclear Medicine
School for Radiological and Interdisciplinary
Sciences (RAD-X)
Soochow University
Suzhou 215123, China
E-mail: zhenli@suda.edu.cn



Dr. J. F. Zeng, Dr. Y. Wang, L. Wen, L. Chen, Prof. Z. Li, Prof. Z. F. Chai
Collaborative Innovation Center of Radiation Medicine of Jiangsu Higher
Education Institutions
Suzhou 215123, China

M. Cheng, Prof. Y. Y. Wu
The Second Affiliated Hospital of Soochow University
Suzhou 215004, China
E-mail: wuyoyo@aliyun.com

Prof. Z. Li
Institute for Superconducting & Electronic Materials
The University of Wollongong
NSW 2500, Australia

Prof. M. Y. Gao
Institute of Chemistry
Chinese Academy of Sciences
Beijing National Laboratory for Molecular Sciences (BNLMS)
Beijing 100190, China
E-mail: gaomy@iccas.ac.cn

DOI: 10.1002/adhm.201500898

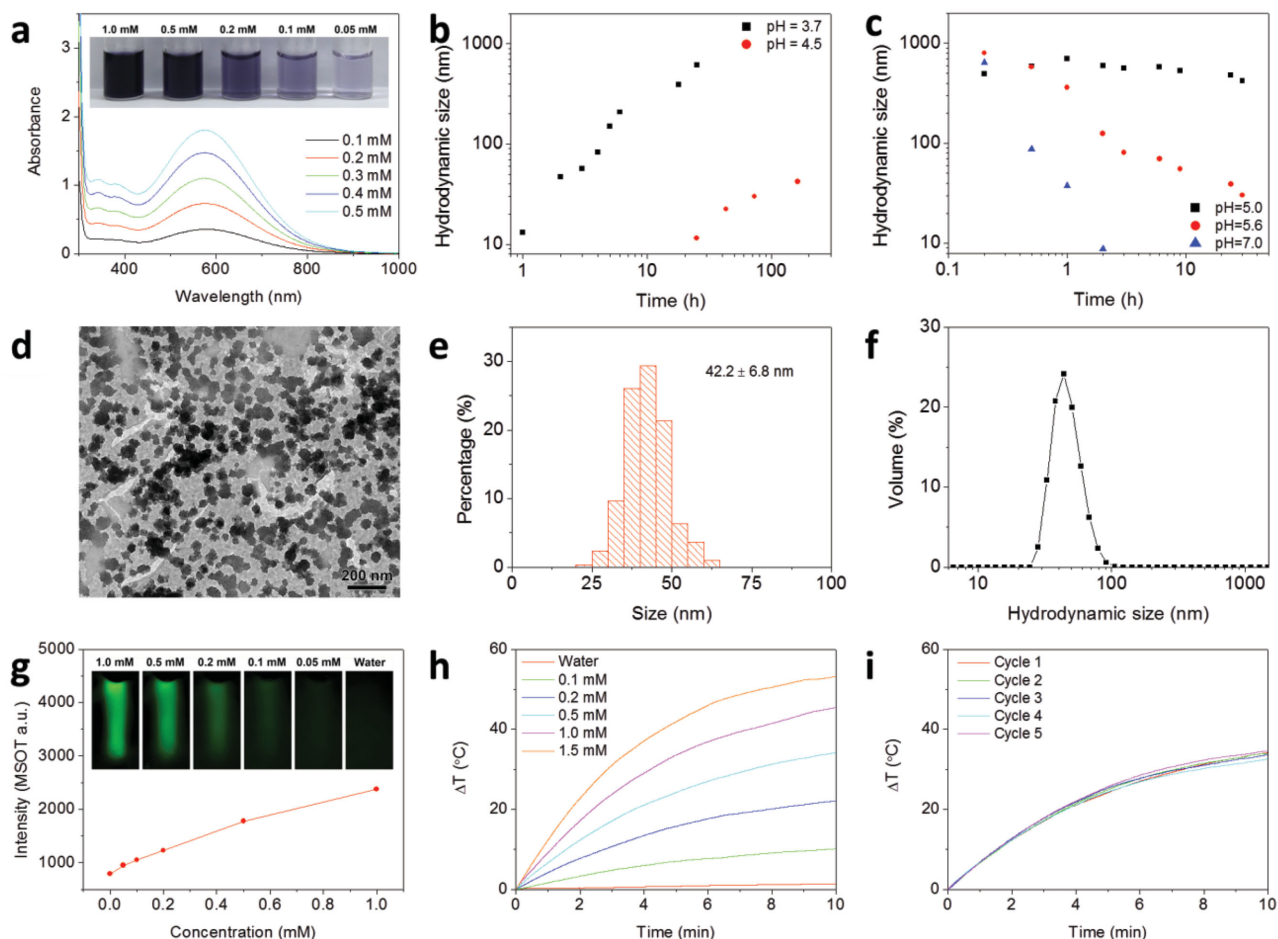


Figure 1. Synthesis and characterization of Fe(III)-gallic acid nanoparticles. a) UV-vis-NIR absorbance spectra of Fe(III)-gallic acid solution. Inset: Photographs of Fe(III)-gallic acid solutions with different iron concentrations. b) Hydrodynamic size evolution of Fe(III)-gallic acid nanoparticles formed under different pH. c) Hydrodynamic size evolution of Fe(III)-gallic acid nanoparticles incubated in aqueous media with different pH. d) TEM image of Fe(III)-gallic acid nanoparticles prepared by mixing FeCl₃ with gallic acid under pH 3.7 for 2 h. e) Corresponding TEM size distribution of Fe(III)-gallic acid nanoparticles displayed in part (d). f) Hydrodynamic size distribution of Fe(III)-gallic acid nanoparticles shown in part (d). g) Photoacoustic signals of Fe(III)-gallic acid nanoparticles at 680 nm as a function of concentration. Inset: Photoacoustic images of different concentrations of Fe(III)-gallic acid nanoparticles in agar phantom. h) Temperature elevation of different concentrations of Fe(III)-gallic acid nanoparticles as a function of irradiation time. i) Temperature variation of Fe(III)-gallic acid nanoparticles (0.5×10^{-3} M) under irradiation for five cycles.

The as-prepared complex solution exhibits strong pH-dependent stability. It is very stable when the solution pH is above 5.0, and no precipitates or particles were detected after one week by dynamic light scattering measurements. When the pH is lower than 5.0, the complex can gradually aggregate and form nanoparticles, as shown in Figure 1b and Figure S1 in the Supporting Information. The hydrodynamic size reaches up to ≈ 45 nm within 72 h at pH 4.5. Decreasing the solution pH from 4.5 to 3.7 leads to fast aggregation and formation of nanoparticles, and their hydrodynamic size reaches ≈ 45 nm within 2 h. The strong pH-dependent stability is closely related to the protonation/deprotonation of carboxyl groups ($-\text{COOH}$) in gallic acid. As the acid dissociation constant (pK_a) of $-\text{COOH}$ in gallic acid is around 4.5, the electrostatic repulsion induced by deprotonation of $-\text{COOH}$ can effectively prevent the aggregation of the Fe(III)-gallic acid complex. When the pH is lower than or equal to the pK_a , however, the electrostatic repulsion decreases significantly, and the hydrophobic

interactions among the complex molecules lead to the formation of Fe(III)-gallic acid nanoparticles. It is worth noting that the aggregation and formation of Fe(III)-gallic acid nanoparticles is reversible. Figure 1c shows the evolution of the hydrodynamic size of Fe(III)-gallic acid nanoparticles incubated in aqueous media with different pH. There is no obvious change in the hydrodynamic size of the Fe(III)-gallic acid nanoparticles when the solution pH is changed from 3.7 to 5.0, indicating the high stability of the thus-formed Fe(III)-gallic acid nanoparticles under acidic conditions. Further increasing the solution pH leads to a gradual decrease in the hydrodynamic size due to the disassembling of Fe(III)-gallic acid nanoparticles into small complex molecules again.

The above results indicate that Fe(III)-gallic acid nanoparticles can directly be obtained by mixing FeCl₃ solution with gallic acid, and the size of the nanoparticles can be easily controlled by adjusting the solution pH and the reaction time. More importantly, the resultant nanoparticles can be directly used

without any further purification. This environmentally friendly method provides a simple way to prepare pH-responsive inorganic/organic nanoparticles for biomedical applications. The resultant Fe(III)–gallic acid nanoparticles are stable at pH of 5.0, but unstable under neutral conditions (pH 7). Their pH-dependent stability suggests that they could be stable in tumors because of the weak acidic microenvironment in tumors, and unstable in other normal tissues, which indicates that they may have a long retention time at tumor sites, but be quickly metabolized in other organs.

In the following study, we used Fe(III)–gallic acid nanoparticles prepared by mixing FeCl₃ with gallic acid under pH 3.7 for 2 h to investigate their potential as a PAI–PTT theranostic agent. The transmission electron microscope (TEM) image shows that they have an average size of 42.6 nm (Figure 1d,e), which is consistent with their hydrodynamic size of 45 nm (Figure 1f). Due to the strong NIR absorption, the Fe(III)–gallic acid nanoparticles show obvious photoacoustic and photothermal effects. As shown in Figure 1g, the photoacoustic signal increases with increasing iron concentration from 0.05×10^{-3} to 1.0×10^{-3} M, indicating that the Fe(III)–gallic acid nanoparticles would be good candidates for PAI. To evaluate their photothermal performance, Fe(III)–gallic acid nanoparticles with various concentrations from 0.1×10^{-3} to 1.5×10^{-3} M were exposed to an 808 nm NIR laser with a power density of 0.5 W cm^{-2} . The temperature of each solution was recorded for 10 min under continuous laser irradiation until the solution reached a steady temperature. As shown in Figure 1h and Figure S2, Supporting Information, the temperature difference (ΔT) drastically increases with the increasing particle concentration. The temperature of the Fe(III)–gallic acid nanoparticle solution with a concentration of 1.5×10^{-3} M can increase by 53°C after irradiation for 10 min. The temperature of pure water was only increased by 2°C under the same conditions. In addition, their photothermal performance remains rather stable after five cycles of NIR laser irradiation (808 nm laser at 0.5 W cm^{-2} , 10 min for each cycle) as shown in Figure 1i. Furthermore, the photothermal conversion efficiency of Fe(III)–gallic acid nanoparticles was calculated to be 66.8% (Figure S3, Supporting Information), which is relatively high compared with those reported for NIR dyes,^[16] gold nanomaterials,^[7b,15] carbon nanomaterials,^[17] transition-metal dichalcogenides,^[2c,8d,18] and polymer nanoparticles.^[14a,19] These results suggest that Fe(III)–gallic acid nanoparticles would be an effective photothermal agent for cancer therapy, as cancer cells can be killed by being kept at 50°C for several minutes.

Considering the excellent photothermal performance of Fe(III)–gallic acid nanoparticles for potential cancer treatment, we further investigated their *in vitro* cytotoxicity and PTT efficacy. The cytotoxicity was evaluated through methyl thiazolyl tetrazolium (MTT) assays on the proliferation of 4T1 cells (murine breast cancer cells). As shown in Figure 2a, the cell viability remained above 80% after incubation with 100×10^{-6} M nanoparticles for 24 h, and 50% of the cells survived at 200×10^{-6} M. To verify their photothermal ablation of cancer cells, 4T1 cells were incubated with Fe(III)–gallic acid nanoparticles at various concentrations for 24 h and then exposed to an irradiation (808 nm) with a power density of 0.5 W cm^{-2} for 10 min. After the irradiation, an MTT assay

was performed to quantitatively determine the cell viability (Figure 2b). The results clearly show that the cell viability decreased drastically with increasing nanoparticle concentration, in comparison with the control groups without NIR laser irradiation (Figure 2a). With a concentration of 200×10^{-6} M, more than 80% of the cells were dead after laser irradiation, suggesting the excellent anticancer performance of these nanoparticles, which was further demonstrated by staining the cells with a Live–Dead Cell Staining Kit after laser irradiation to differentiate the live and dead cells. Most cells were destroyed after incubation with 200×10^{-6} M Fe(III)–gallic acid nanoparticles and exposure to irradiation with a 808 nm laser (Figure 2c). In contrast, only few cells died if they were not incubated with Fe(III)–gallic acid nanoparticles and/or not exposed to laser irradiation. These results demonstrate that Fe(III)–gallic acid nanoparticles could serve as a potential PTT agent for photothermal ablation of cancer cells.

As mentioned previously, PTT agents could also serve as contrast agents for photoacoustic imaging. To further demonstrate the potential of Fe(III)–gallic acid nanoparticles in tumor imaging, a subcutaneously transplanted 4T1 tumor model was adopted. BALB/c nude mice with different tumor sizes of 5–10 mm were selected to evaluate the photoacoustic (PA) imaging performance of Fe(III)–gallic acid nanoparticles (4×10^{-3} M, 200 μL for each mouse), which were intravenously injected through the tail vein. A set of PA images of the tumor region acquired before and at different time points post-injection are presented in Figure 3a. The overall contrast of the tumor area was gradually enhanced after injection of Fe(III)–gallic acid nanoparticles, indicating a continuing accumulation of nanoparticles in the tumor area via blood circulation. The accumulation of nanoparticles at the tumor site could be attributed to the EPR effect, which is a common mechanism for passive targeting of nanoparticles. It is reasonable to expect the accumulation of our nanoparticles at the tumor site because their size is suitable for the EPR effect. In addition, the signal enhancement is more pronounced for large tumors, demonstrating that nanoparticles could be more effectively taken up by large tumors than smaller ones. This is expected, because large tumors may have more tumor blood vessels that would give rise to a stronger EPR effect than in the smaller tumors. These results demonstrate that Fe(III)–gallic acid nanoparticles are an excellent photoacoustic imaging agent, which can significantly illuminate the tumor and clearly delineate the margin of the tumor.

To further quantitatively evaluate the performance of the Fe(III)–gallic acid nanoparticles, the PA signals of the region of interest in each image were calculated and are presented in Figure 3b. The quantified results reveal that, for all different sized tumors, Fe(III)–gallic acid nanoparticles produce increased contrast at the tumor site in the first 4 h post-injection, so that the contrast reaches its maximum value at around 8 h, and then slightly decreases with the circulation time. The signal enhancement is more pronounced in large tumors than smaller ones, which is consistent with the images shown in Figure 3a. Furthermore, the results also suggest that the optimal time for irradiation would be 8 h after injection of Fe(III)–gallic acid nanoparticles, at which the maximum accumulation of nanoparticles at the tumor site and their best PTT efficacy could be

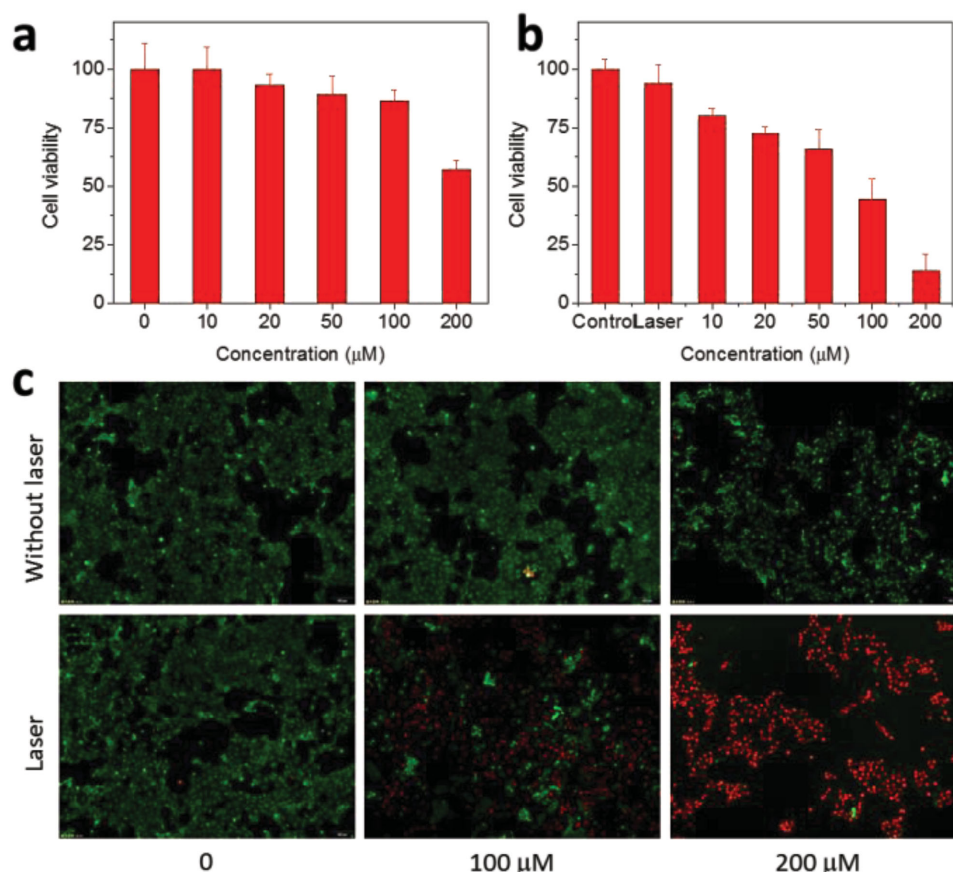


Figure 2. In vitro cell experiments. a) Relative cell viabilities of 4T1 cells after being incubated with various concentration of Fe(III)-gallic acid nanoparticles for 24 h. b) Relative cell viabilities of 4T1 cells incubated with various concentration of Fe(III)-gallic acid nanoparticles under 808 nm laser irradiation (0.5 W cm^{-2} , 10 min). c) Live-Dead Cell Staining Kit stained images of 4T1 cells incubated with Fe(III)-gallic acid nanoparticles at different concentrations after laser irradiation for 10 min at a power density of 0.5 W cm^{-2} .

obtained. The effects of PA enhancement on different sized tumors are further demonstrated by comparison of the tumor signal obtained pre-injection with the maximum value obtained after injection (Figure 3c). Compared with the PA signal of the tumor site itself, the accumulation of Fe(III)-gallic acid nanoparticles could increase the signal by 61%, 235%, and 403%, respectively, for different sized tumors. Figure 3c also shows that a large tumor has a stronger PA signal than the smaller ones. As the PA signal of the tumor site obtained pre-injection is positively related to the blood content of tumor tissue, the above result suggests that a large tumor would have richer tumor blood vessels, which leads to a stronger EPR effect for the uptake of Fe(III)-gallic acid nanoparticles.

Encouraged by the promising in vitro photothermal ablation effect on cancer cells and the in vivo PAI imaging of tumors, we further evaluated the photothermal effect of Fe(III)-gallic acid nanoparticles in vivo. According to the above in vivo PAI results, mice bearing 4T1 tumors with different sizes were anesthetized after intravenous (IV) injection of Fe(III)-gallic acid nanoparticles ($4 \times 10^{-3} \text{ M}$, 200 μL for each mouse) for 8 h, which is the optimal time for accumulation of nanoparticles in a tumor, and then exposed to 808 nm irradiation with a power density of 1.0 W cm^{-2} . An infrared imaging camera was used to monitor the temperature changes in the tumor

site under NIR irradiation. The temperature of the tumor area increased by 9.9, 19.8, and 24.4°C within 10 min under laser irradiation for mice with tumor sizes of 60, 150, and 260 mm^3 (Figure 3d,e), respectively. In comparison, the tumor temperature of mice from the control group (i.e., intravenous injection of saline and then the same irradiation conditions) was only increased by 5.5°C , much lower than for the mice injected with Fe(III)-gallic acid nanoparticles. In addition, large tumors exhibited higher temperature than small ones. This should be attributed to more efficient uptake of Fe(III)-gallic acid nanoparticles by large tumors than smaller ones through the EPR effect. The consistency between the PTT and the PAI results suggests that the PA imaging can serve as an effective method to guide the photothermal ablation of tumors. The results also indicate the difficulty in photothermal ablation of small tumors due to less accumulation of nanoparticles in the tumor (i.e., less passive targeting of nanoparticles through the EPR effect). Nevertheless, for a tumor with a size of 150 mm^3 in the current study, the increased temperature ($\Delta T = 19.8^\circ\text{C}$) would be high enough to ablate it in vivo. This size is comparable to those of tumors used for many PTT studies in the literature.^[8b,20]

As photoacoustic imaging can also serve as a noninvasive imaging technique for semiquantifying the pharmacokinetics of drugs, we conducted a preliminary evaluation of the

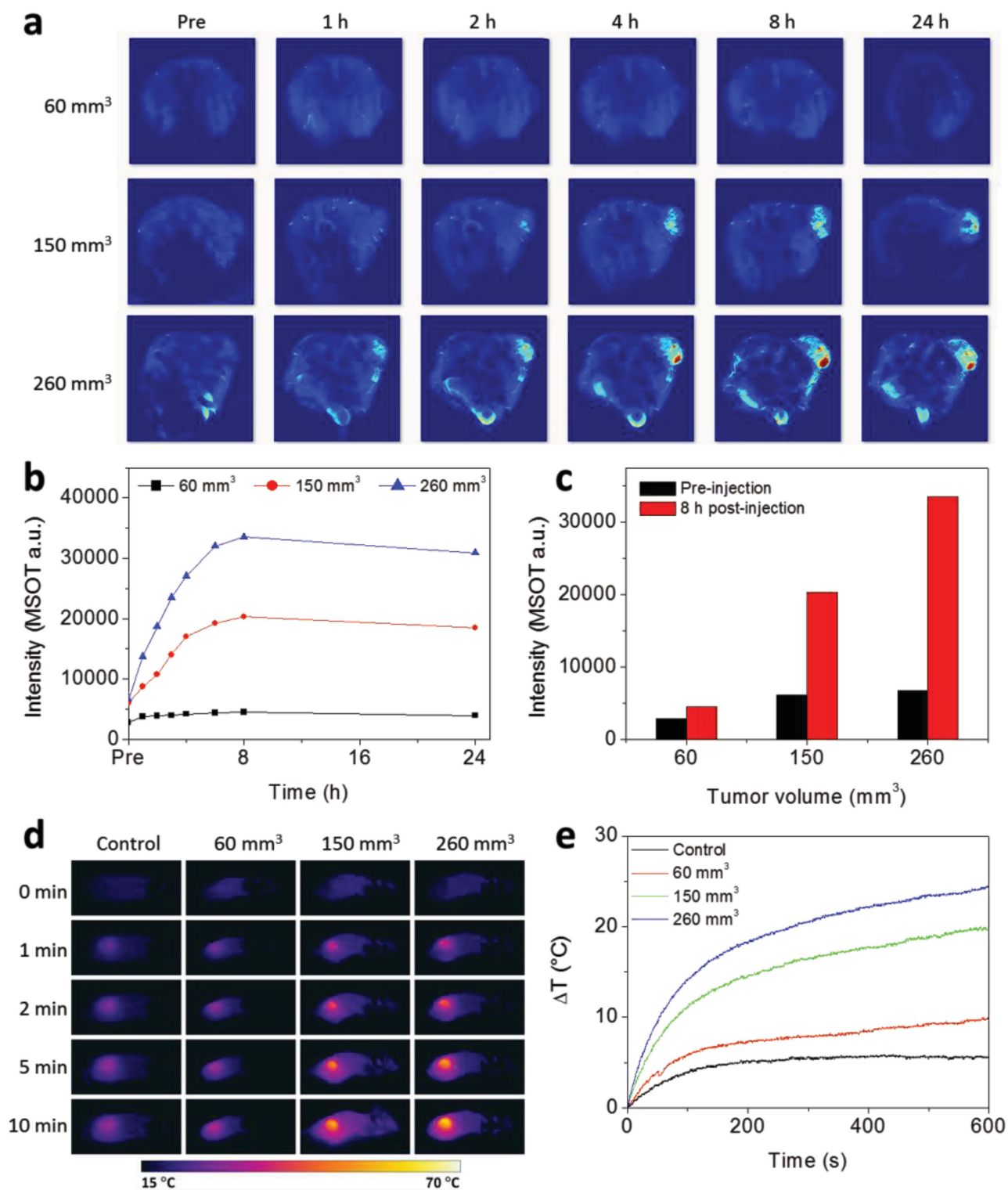


Figure 3. In vivo photoacoustic imaging and photothermal effect of Fe(III)-gallic acid nanoparticles. a) Photoacoustic images of mice bearing different sized tumors before injection and at different time points post-injection with Fe(III)-gallic acid nanoparticles. b) Photoacoustic signal variations of tumor sites in part (a) as a function of post-injection time. c) Photoacoustic signals of different sized tumors before injection and 8 h post-injection of Fe(III)-gallic acid nanoparticles. d) Thermal images of mice bearing different sized tumors after injection of saline (column 1) or Fe(III)-gallic acid nanoparticles (columns 2–4) in combination with exposure to 808 nm laser irradiation (1.0 W cm⁻², 10 min). e) Tumor temperature changes in mice bearing different sized tumors during laser irradiation as indicated in part (d).

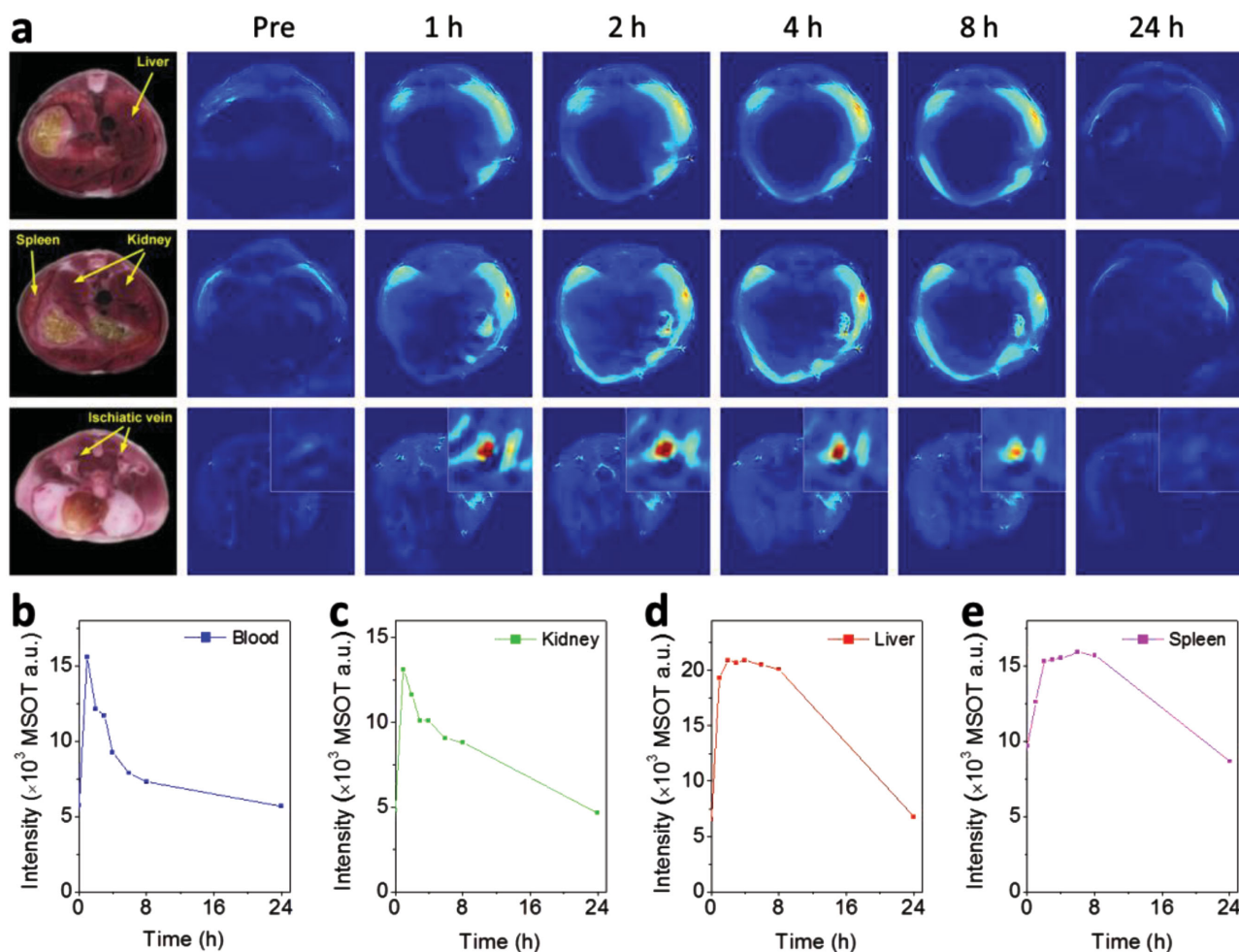


Figure 4. In vivo biodistribution and clearance of Fe(III)-gallic acid nanoparticles. a) In vivo photoacoustic images of liver, spleen, kidney, and ischiatic vein after the intravenous injection of Fe(III)-gallic acid nanoparticles at different time intervals. b–e) Photoacoustic signals of blood, kidney, liver, and spleen, respectively, as a function of time post-injection of Fe(III)-gallic acid nanoparticles. MSOT: Multispectral optoacoustic tomography.

pharmacokinetics of Fe(III)-gallic acid nanoparticles in mice by using the PAI method. **Figure 4a** displays the PA images of major organs of nude mice before and after injection of Fe(III)-gallic acid nanoparticles. The PA signals of each organ were calculated and are presented in **Figure 4b–e**. The signal change in the ischiatic vein was used to demonstrate the variation in the content of Fe(III)-gallic acid nanoparticles in the blood. After injection of Fe(III)-gallic acid nanoparticles, the PA signal in the blood increased significantly and then gradually decreased, indicating the clearance of Fe(III)-gallic acid nanoparticles from the blood. The PA signal of blood after 8 h is higher than that pre-injection, suggesting a long blood circulation time of Fe(III)-gallic acid nanoparticles. The retention time of Fe(III)-gallic acid nanoparticles in blood is much longer than the decomposition time of nanoparticles under the neutral condition, as shown in **Figure 1c**. This is due to the complicated environment and the protection provided by proteins in blood, which is evidenced by the slow degradation of Fe(III)-gallic acid nanoparticles in 10% fetal bovine serum (FBS) in **Figure S4**, Supporting Information. Although the decomposition of Fe(III)-gallic acid nanoparticles in FBS is slower, they can be

almost completely decomposed within one day, indicating the fast metabolic breakdown of Fe(III)-gallic acid nanoparticles. The PA signal of the kidney shows a similar trend to that in the blood, but the signal decreased much more slowly than the decay observed for blood, suggesting that renal excretion may be one of the metabolic pathways for Fe(III)-gallic acid nanoparticles. The PA signals of the liver and spleen dramatically increased after 1 h post-injection, indicating the fast accumulation of Fe(III)-gallic acid nanoparticles in the liver and spleen. This is expected, as nanoparticles are easily captured by the reticuloendothelial system, leading to the strong PA signal. The PA signals of the liver and spleen reached an approximate plateau after 2 h, and then gradually decreased from 4 h and 6 h, respectively. After 24 h, the PA signal of the liver and spleen recovered to the pre-injection level, indicating that the Fe(III)-gallic acid nanoparticles in these organs may be gradually decomposed into small molecular complexes and then easily excreted from the treated animals. In remarkable contrast, the Fe(III)-gallic acid nanoparticles were still accumulating in the tumor after 24 h post-injection, as shown in **Figure 3**. The above results fully demonstrate that Fe(III)-gallic acid

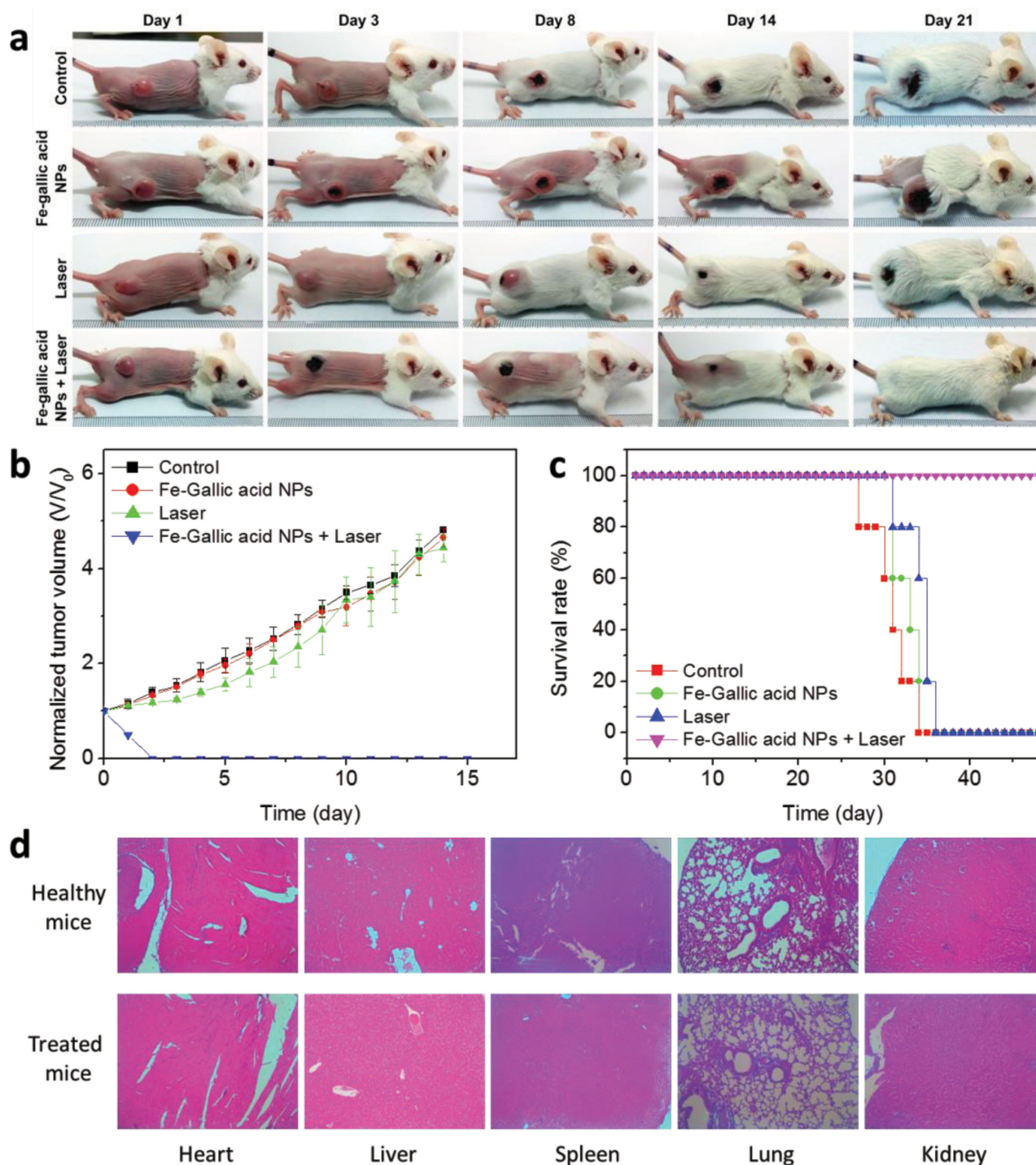


Figure 5. In vivo photothermal therapy using Fe(III)-gallic acid nanoparticles. a) Representative photographs of mice bearing 4T1 tumors after the various different treatments indicated. b) Corresponding growth curves of 4T1 tumors in different groups of mice after treatment. The relative tumor volumes were normalized to their initial size. c) Survival curves of mice after various treatments as indicated. d) H&E stained images of major organs from untreated healthy mice and treated mice with Fe(III)-gallic acid nanoparticle injection, taken 45 d after photothermal therapy (with tumors eliminated).

nanoparticles can be easily decomposed in the liver and spleen while remaining stable in the tumor with a long retention time. In addition, the clearance of Fe(III)-gallic acid nanoparticles in vivo takes place more quickly than for other nanomaterials studied in the literature,^[8a,21] demonstrating that Fe(III)-gallic

acid nanoparticles could be a safe and promising candidate as a PAI-PTT theranostic agent.

To assess the in vivo therapeutic potential of Fe(III)-gallic acid nanoparticles, a further careful investigation of their photothermal therapeutic efficacy was carried out. Balb/c mice with

subcutaneous 4T1 tumors were selected as the animal model. After the tumor sizes reached approximately 150 mm³, the mice were divided into four groups with five mice per group. For the treatment group, they were intravenously injected with Fe(III)-gallic acid nanoparticles (4×10^{-3} M, 200 μ L for each mouse). After 8 h, their tumors were irradiated by an 808 nm laser for 10 min with a power density of 1 W cm⁻². The other three groups included the saline injection group, a group in which the mice were injected with saline and also exposed to the laser, and a group in which the mice were injected with Fe(III)-gallic acid nanoparticles, but without laser irradiation. The tumor sizes were measured every day after treatment. For the treatment group, the tumor shrank remarkably after 1 d of photothermal treatment, and black scars were formed, which were completely eradicated 14 d after treatment (Figure 5a). In contrast, for the other three control groups, neither the laser irradiation with the current power density nor Fe(III)-gallic acid nanoparticles alone could affect the tumor growth (Figure 5b). In addition, the mice in the control groups had an average lifespan of 30–33 d, shorter than for the treated mice, which were tumor free after treatment and sacrificed on purpose after living for 45 d (Figure 5c). The above results suggest that Fe(III)-gallic acid nanoparticles could serve as a powerful PTT agent for in vivo photothermal ablation of cancer.

To further demonstrate the in vivo toxicity of Fe(III)-gallic acid nanoparticles, the treated mice were sacrificed 45 d after treatment, and the major organs were collected, sliced, and stained by hematoxylin and eosin for histological analysis (Figure 5d). Compared with the normal mice, no noticeable inflammation or damage was observed in any of the major organs. The results indicate that Fe(III)-gallic acid nanoparticles are not toxic to mice with the current experimental dosage. In addition, as the spread of cancer cells into the lung is the main metastasis of 4T1 tumors, Figure 5d also shows no appreciable signs of pulmonary metastasis for surviving mice with tumors that were photothermally ablated.

In summary, a new type of PAI-PTT nanotheranostic agent based on pH-sensitive Fe(III)-gallic acid complex was successfully developed. The complex has a strong NIR absorbance and can reversibly aggregate into nanoparticles with a size that is controllable by simply changing the solution pH value. The resultant nanoparticles are stable under mild acidic conditions (pH around 5.0) and unstable under neutral pH, which is perfectly suitable for cancer diagnosis and treatment, because the nanoparticles would be stable in the weak acidic environment of a tumor, while being easily metabolized in other organs. In vitro experiments show that the Fe(III)-gallic acid nanoparticles present low toxicity and excellent photothermal ablation of cancer cells, so that they can serve as an efficient photothermal agent. Further in vivo PAI and PTT experiments showed that Fe(III)-gallic acid nanoparticles are accumulated more in large tumors than in small ones because of the stronger EPR effect in the larger tumors. The results also suggest that PAI can be employed to guide the photothermal ablation of tumors. The pharmacokinetics results show that Fe(III)-gallic acid nanoparticles have longer retention times in tumors than in the liver and spleen, where they can be easily degraded and excreted, due to their pH sensitivity. The in vivo treatment results demonstrate that Fe(III)-gallic acid nanoparticles are a highly

effectively photothermal agent for NIR light-induced tumor ablation. In addition, no acute toxicity was observed for the Fe(III)-gallic acid nanoparticles in our experiments, demonstrating their excellent biocompatibility. Our research provides a new strategy for designing theranostic agents for cancer diagnosis and treatment through PAI/PTT

Supporting Information

Supporting Information is available from the Wiley Online Library or from the author.

Acknowledgements

J. Zeng and M. Cheng contributed equally to this work. This work was partially supported by the National Natural Science Foundation of China (81471657, 81530057, and 21503141), Beijing National Laboratory for Molecular Sciences (20140165), and China Postdoctoral Science Foundation (2015M570472). Z. Li acknowledges the support from the program of Jiangsu Specially Appointed Professorship. The authors also thank Dr. Tania Silver for polishing the manuscript.

Received: November 6, 2015

Published online: February 4, 2016

- [1] a) Y. Chen, C. Tan, H. Zhang, L. Wang, *Chem. Soc. Rev.* **2015**, *44*, 2681; b) K. Yang, L. Z. Feng, X. Z. Shi, Z. Liu, *Chem. Soc. Rev.* **2013**, *42*, 530; c) E. Terreno, F. Uggeri, S. Aime, *J. Controlled Release* **2012**, *161*, 328.
- [2] a) J. Li, Y. Hu, J. Yang, P. Wei, W. Sun, M. Shen, G. Zhang, X. Shi, *Biomaterials* **2015**, *38*, 10; b) X. Song, H. Gong, S. Yin, L. Cheng, C. Wang, Z. Li, Y. Li, X. Wang, G. Liu, Z. Liu, *Adv. Funct. Mater.* **2014**, *24*, 1194; c) Q. Tian, J. Hu, Y. Zhu, R. Zou, Z. Chen, S. Yang, R. Li, Q. Su, Y. Han, X. Liu, *J. Am. Chem. Soc.* **2013**, *135*, 8571.
- [3] J. Lin, S. Wang, P. Huang, Z. Wang, S. Chen, G. Niu, W. Li, J. He, D. Cui, G. Lu, X. Chen, Z. Nie, *ACS Nano* **2013**, *7*, 5320.
- [4] a) Y. Chen, D. L. Ye, M. Y. Wu, H. R. Chen, L. L. Zhang, J. L. Shi, L. Z. Wang, *Adv. Mater.* **2014**, *26*, 7019; b) E.-K. Lim, Y.-M. Huh, J. Yang, K. Lee, J.-S. Suh, S. Haam, *Adv. Mater.* **2011**, *23*, 2436.
- [5] Z. Zhou, B. Kong, C. Yu, X. Shi, M. Wang, W. Liu, Y. Sun, Y. Zhang, H. Yang, S. Yang, *Sci. Rep.* **2014**, *4*, 3653.
- [6] D. Chen, C. Wang, X. Nie, S. Li, R. Li, M. Guan, Z. Liu, C. Chen, C. Wang, C. Shu, L. Wan, *Adv. Funct. Mater.* **2014**, *24*, 6621.
- [7] a) J. C. Ge, Q. Y. Jia, W. M. Liu, L. Guo, Q. Y. Liu, M. H. Lan, H. Y. Zhang, X. M. Meng, P. F. Wang, *Adv. Mater.* **2015**, *27*, 4169; b) P. Huang, J. Lin, W. Li, P. Rong, Z. Wang, S. Wang, X. Wang, X. Sun, M. Aronova, G. Niu, R. D. Leapman, Z. Nie, X. Chen, *Angew. Chem. Int. Ed.* **2013**, *52*, 13958; c) J. C. Ge, M. H. Lan, B. J. Zhou, W. M. Liu, L. Guo, H. Wang, Q. Y. Jia, G. L. Niu, X. Huang, H. Y. Zhou, X. M. Meng, P. F. Wang, C. S. Lee, W. J. Zhang, X. D. Han, *Nat. Commun.* **2014**, *5*; d) P. Huang, P. F. Rong, J. Lin, W. W. Li, X. F. Yan, M. G. Zhang, L. M. Nie, G. Niu, J. Lu, W. Wang, X. Y. Chen, *J. Am. Chem. Soc.* **2014**, *136*, 8307.
- [8] a) K. Yang, G. Yang, L. Chen, L. Cheng, L. Wang, C. Ge, Z. Liu, *Biomaterials* **2015**, *38*, 1; b) J. Yu, C. Yang, J. Li, Y. Ding, L. Zhang, M. Z. Yousaf, J. Lin, R. Pang, L. Wei, L. Xu, F. Sheng, C. Li, G. Li, L. Zhao, Y. Hou, *Adv. Mater.* **2014**, *26*, 4114; c) Q. Tian, Q. Wang, K. X. Yao, B. Teng, J. Zhang, S. Yang, Y. Han, *Small* **2014**, *10*, 1063; d) W. Yin, L. Yan, J. Yu, G. Tian, L. Zhou, X. Zheng, X. Zhang,

- Y. Yong, J. Li, Z. Gu, Y. Zhao, *ACS Nano* **2014**, *8*, 6922; e) D. Jaque, L. Martínez Maestro, B. del Rosal, P. Haro-Gonzalez, A. Benayas, J. L. Plaza, E. Martín Rodríguez, J. García Sole, *Nanoscale* **2014**, *6*, 9494; f) L. M. Nie, X. Y. Chen, *Chem. Soc. Rev.* **2014**, *43*, 7132.
- [9] A. Yuan, J. H. Wu, X. L. Tang, L. L. Zhao, F. Xu, Y. Q. Hu, *J. Pharm. Sci.* **2013**, *102*, 6.
- [10] a) J. Shen, H.-C. Kim, C. Mu, E. Gentile, J. Mai, J. Wolfram, L.-N. Ji, M. Ferrari, Z.-W. Mao, H. Shen, *Adv. Healthcare Mater.* **2014**, *3*, 1629; b) J.-G. Piao, L. Wang, F. Gao, Y.-Z. You, Y. Xiong, L. Yang, *ACS Nano* **2014**, *8*, 10414.
- [11] a) Y. Wang, K. Wang, J. Zhao, X. Liu, J. Bu, X. Yan, R. Huang, *J. Am. Chem. Soc.* **2013**, *135*, 4799; b) X. Shi, H. Gong, Y. Li, C. Wang, L. Cheng, Z. Liu, *Biomaterials* **2013**, *34*, 4786.
- [12] L. Cheng, K. Yang, Y. Li, J. Chen, C. Wang, M. Shao, S.-T. Lee, Z. Liu, *Angew. Chem. Int. Ed.* **2011**, *50*, 7385.
- [13] L. Cheng, J. Liu, X. Gu, H. Gong, X. Shi, T. Liu, C. Wang, X. Wang, G. Liu, H. Xing, W. Bu, B. Sun, Z. Liu, *Adv. Mater.* **2014**, *26*, 1886.
- [14] a) M. Chen, X. Fang, S. Tang, N. Zheng, *Chem. Commun.* **2012**, *48*, 8934; b) L. Cheng, K. Yang, Q. Chen, Z. Liu, *ACS Nano* **2012**, *6*, 5605.
- [15] X. Ding, C. H. Liow, M. Zhang, R. Huang, C. Li, H. Shen, M. Liu, Y. Zou, N. Gao, Z. Zhang, Y. Li, Q. Wang, S. Li, J. Jiang, *J. Am. Chem. Soc.* **2014**, *136*, 15684.
- [16] M. Zheng, P. Zhao, Z. Luo, P. Gong, C. Zheng, P. Zhang, C. Yue, D. Gao, Y. Ma, L. Cai, *ACS Appl. Mater. Interfaces* **2014**, *6*, 6709.
- [17] J. Q. Chen, X. P. Wang, T. S. Chen, *Nanoscale Res. Lett.* **2014**, *9*, 86.
- [18] J. Liu, X. P. Zheng, L. Yan, L. J. Zhou, G. Tian, W. Y. Yin, L. M. Wang, Y. Liu, Z. B. Hu, Z. J. Gu, C. Y. Chen, Y. L. Zhao, *ACS Nano* **2015**, *9*, 696.
- [19] J. Zhou, Z. Lu, X. Zhu, X. Wang, Y. Liao, Z. Ma, F. Li, *Biomaterials* **2013**, *34*, 9584.
- [20] a) C. Yue, P. Liu, M. Zheng, P. Zhao, Y. Wang, Y. Ma, L. Cai, *Biomaterials* **2013**, *34*, 6853; b) H. Gong, Z. Dong, Y. Liu, S. Yin, L. Cheng, W. Xi, J. Xiang, K. Liu, Y. Li, Z. Liu, *Adv. Funct. Mater.* **2014**, *24*, 6492; c) M. Guo, H. Mao, Y. Li, A. Zhu, H. He, H. Yang, Y. Wang, X. Tian, C. Ge, Q. Peng, X. Wang, X. Yang, X. Chen, G. Liu, H. Chen, *Biomaterials* **2014**, *35*, 4656.
- [21] a) L. Cheng, K. Yang, M. W. Shao, X. H. Lu, Z. Liu, *Nanomedicine* **2011**, *6*, 1327; b) W.-S. Cho, M. Cho, J. Jeong, M. Choi, B. S. Han, H.-S. Shin, J. Hong, B. H. Chung, J. Jeong, M.-H. Cho, *Toxicol. Appl. Pharm.* **2010**, *245*, 116; c) J. F. Zeng, B. Jia, R. R. Qiao, C. Wang, L. H. Jing, F. Wang, M. Y. Gao, *Chem. Commun.* **2014**, *50*, 2170; d) C. Y. Liu, Z. Y. Gao, J. F. Zeng, Y. Hou, F. Fang, Y. L. Li, R. R. Qiao, L. Shen, H. Lei, W. S. Yang, M. Y. Gao, *ACS Nano* **2013**, *7*, 7227.